Superelastic behavior of single crystalline $Ni_{48}Fe_{20}Co_5Ga_{27}$ micro-pillars near austenite–martensite critical point

Cite as: AIP Advances **11**, 025213 (2021); https://doi.org/10.1063/5.0036304
Submitted: 03 November 2020 . Accepted: 07 January 2021 . Published Online: 04 February 2021

T.-F. M. Chang, V. Chernenko, H.-C. Tang, C.-Y. Chen, A. Umise, M. Tahara, H. Hosoda, and M. Sone

Superelastic behavior of single crystalline $Ni_{48}Fe_{20}Co_5Ga_{27}$ micro-pillars near austenite–martensite critical point

Cite as: AIP Advances 11, 025213 (2021); doi: 10.1063/5.0036304
Submitted: 3 November 2020 • Accepted: 7 January 2021 •
Published Online: 4 February 2021

T.-F. M. Chang,[1,a] V. Chernenko,[1,2,3,a] H.-C. Tang,[1] C.-Y. Chen,[1] A. Umise,[1,4] M. Tahara,[1] H. Hosoda,[1] and M. Sone[1]

AFFILIATIONS

[1] Institute of Innovative Research, Tokyo Institute of Technology, Nagatsuta, Midori-ku 4259, Yokohama 226-8503, Japan
[2] BCMaterials and University of Basque Country, UPV/EHU, Bilbao 48080, Spain
[3] Ikerbasque, Basque Foundation for Science, Bilbao 48009, Spain
[4] Institute of Biomaterials and Bioengineering, Tokyo Medical and Dental University, 1-5-45 Yushima, Bunkyo-ku, Tokyo 101-0062, Japan

[a] **Authors to whom correspondence should be addressed:** chang.m.aa@m.titech.ac.jp and vladimir.chernenko@gmail.com

ABSTRACT

Micro-pillars oriented in austenite along [100], [110], and [111] crystallographic directions were fabricated on the corresponding edges of a single crystalline plate of the $Ni_{48}Fe_{20}Co_5Ga_{27}$ magnetic shape memory alloy exhibiting martensitic transformation (MT) at 150 K. Superelastic behavior of pillars, due to micro-compression-induced MT, was investigated at different temperatures from 298 K to 373 K. At room temperature, Young's moduli of the [100], [110], and [111] pillars in austenite are equal to 5.3 GPa, 7.9 GPa, and 9.9 GPa, respectively, resulting in the linear dependences of the elastic strain reaching up to the record-breaking value of 10%. On increasing temperature, the stress–strain dependencies exhibit changes that are interpreted in terms of the critical behavior on approaching to the end points on the martensite–austenite stress–temperature phase diagrams.

Superplasticity (pseudoelasticity) is both the fundamental phenomenon and important functionality exhibited by the shape memory alloys (SMAs).[1,2] Its origin lies on the reversible stress-induced martensitic transformation (MT), which proceeds by a lattice distortion of the initial cubic austenite resulting in a formation of the lower symmetry (usually, tetragonal) martensitic phase. Different values of the stresses needed to start the forward and to finish the reverse MT reflect the stress hysteresis of MT, revealing its first-order character. The stress/temperature evolutions of the MT hysteresis toward its disappearance in the critical point, CP, (end point on the stress–temperature phase diagram of MT with coordinates T^*, σ^*) have been recently discovered experimentally and explained theoretically in Ni–Fe(Co)–Ga and Fe–Pd magnetic shape memory single crystals (see Ref. 3 and references therein). Above CP, where MT does not exist anymore, a hysteresisless postcritical behavior of the functional properties was found,[4] suggesting an important avenue to be pursued toward the high-tech applications, such as nanobeam actuators[5] or elastocaloric devices.[6]

Previous studies revealed that the characteristics of stress-induced MT in SMAs, such as the martensite start stress, σ_{MS}, and its temperature variation, depend on the crystal lattice orientation (see, e.g., Refs. 7 and 8) and dimensions of the specimen,[6,9,10] either of these, in turn, affects the related functionalities of SMAs. Particularly, there are several reports about the microscaling effects on the superelastic (SE) and shape memory characteristics in magnetic SMAs, but due to the technical limitations, the phase diagrams of "σ_{MS} vs temperature" have not been studied yet.[11,12] This is one of the reasons why the critical behavior and existence of the end points in the phase diagrams have been unexplored

yet on the microscale. In addition, no reports about orientation dependence of the critical characteristics are found in the literature. In order to fill these gaps, in the present work, the micro-pillars with three different crystallographic orientations were prepared using corresponding edges of the $Ni_{48}Fe_{20}Co_5Ga_{27}$ single crystalline plate and their superelastic (SE) stress–strain dependences were tested at different constant temperatures. As a result, the huge linear reversible strains and the approximate locations of CPs were identified.

Master alloy with a nominal composition of $Ni_{48}Fe_{20}Co_5Ga_{27}$ (at. %) was fabricated by arc melting the high purity elements and homogenized. The single crystal was grown in a floating zone furnace. It was heat treated at 1173 K during 72 h under argon atmosphere and quenched into water. The chemical composition of $Ni_{48.3}Fe_{20.2}Co_{5.2}Ga_{26.3}$ (at. %) was determined with an uncertainty of 0.5 at. % by the energy dispersive x-ray spectroscopy. The low-field thermomagnetization curve revealed the MT temperature of $T_{ms} \approx 150$ K, in which the $L2_1$-ordered cubic austenite starts to transform into a tetragonal nonmodulated martensite with $c/a > 1$.[3,4,13] A thin polished plate measuring 1 cm × 0.5 cm × 5 μm was cut from the single crystal, and its crystallographic directions were identified by electron backscattered diffraction (EBSD) with e-Flash Bruker AXS, attached to a scanning electron microscope (SEM, S-4300SE Hitachi). Micro-pillars with three crystallographic orientations of [100], [110], and [111] and a dimension of 20 × 20 × 40 μm^3 were fabricated using the corresponding edges of the plate by a focused ion beam (FIB, FB2100 Hitachi) with ion irradiation parallel to the pillar axis to prevent the tapering effect[14] (the details can be found elsewhere[15,16]). It is worth noting that each face of the pillar was finally polished with a low current beam to remove damaged layers and make surfaces smooth. After the FIB process, crystallographic orientations of the micro-pillars were reconfirmed by EBSD.

Micro-compression tests were carried out using a custom-made machine.[17] The test was conducted at a constant displacement rate of 0.1 μm/s using a piezoelectric actuator. The displacement and the applied force were recorded by using an AC/DC converter. Temperature control during the compression test was realized by placing the sample holder between two heaters. The thermocouple was in contact with the sample holder. Each "loading/unloading" cycle was performed at a given fixed temperature, which was varied between 298 K and 393 K.

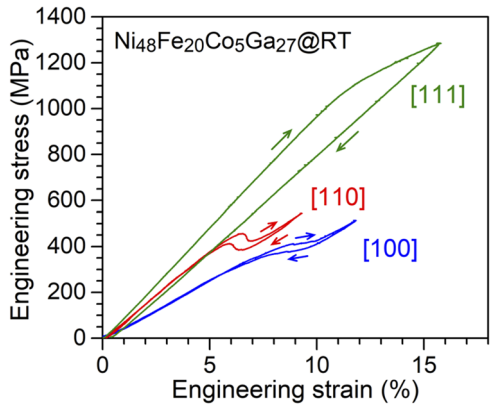

FIG. 1. Compression stress–strain curves for three pillars measured at 298 K.

TABLE I. Young's modulus of the $Ni_{48}Fe_{20}Co_5Ga_{27}$ (at. %) pillars in a cubic phase estimated from the data in Fig. 1.

Pillar (hkl)	Young's modulus, $E_{(hkl)}$, (GPa)
[100]	5.3
[110]	7.9
[111]	9.9

The results of the micro-compression tests are presented in Figs. 1–3. The mechanical tests at room temperature provide a remarkable behavior of the pillars, which can be traced from the stress–strain curves shown in Fig. 1. The dependences in Fig. 1 demonstrate elastic characteristics hardly observable in the bulk state of similar alloys, if referred to a huge linear deformation in the austenitic state before start of the stress-induced MT and high value of stress (more than 1 GPa) at which the pillar is still able to survive. The value of elastic deformation of austenite is equal to about 5%, 7% and 10% for [110], [100], and [111] pillars, respectively. Such huge values of elastic strains at 298 K are the result of both the extremely low values of Young's modulus of pillars, $E_{[hkl]}$, listed in Table I [also observed in the bulk Ni–Fe(Ga)–Co single crystals[4,13]] and a big difference between 298 K and $T_{ms} \approx 150$ K implying a weak temperature dependence of $E_{[hkl]}$ and high value of σ_{MS}. This is a unique behavior compared to that of the Fe_3Pt bulk single crystal, where a much lower value of $E_{[100]} \approx 1.7$ GPa at 90 K (just above T_{ms}) but its much higher value at room temperature, of about 50 GPa, were observed,[18] meaning a strong thermally induced elevation of $E_{[100]}$. Besides, the high values of elastic strains and enhanced strength of studied pillars have also been expected due to the presumed low concentration or lack of defects.

After elastic deformation in austenite, the curves for [100] and [110] pillars in Fig. 1 exhibit the plateau-like hysteretic anomalies produced by the stress-induced MT, whereas in [111] pillar the appearance of MT is masked by a strain hardening. The hysteretic stress–strain loops are the common signatures of the conventional superelastic effect and first-order character of MT. Moreover, in the case of [110] orientation, the stress minimum on the curve reflects a nonequilibrium process related to the specific nucleation-growth pass of martensitic phase, which is an additional evidence of the first-order character of MT. The modeling shows that the slope of the plateau on the SE curve is controlled by both the rate of phase formation and the relative values of stiffness coefficients of the two phases, resulting in the monotone stress–strain dependencies when compressed along the [100] axis and in the negative slopes of the plateaus under a compression along the [110] axis.[19]

As already mentioned, the results of the first compression test of the [111] pillar (Fig. 1) indicate some strain hardening. The hardening is obviously produced by the formation of the dislocations and their accumulation, whereby a material exhibits a plastic deformation. The second stress–strain cycle shown in Fig. 2(a) and images in Fig. 2(b) confirm a high room temperature ductility of pillar, which

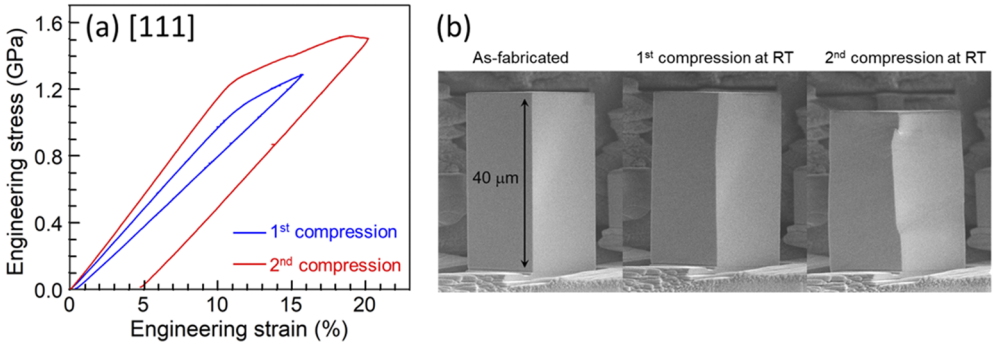

FIG. 2. (a) Compression stress–strain curves for the [111] micro-pillar tested two times at 298 K. (b) SEM images of this pillar showing the plastic deformation after the second compression.

can be spotted by a residual strain of 5% and enhanced yield stress in comparison to the first cycle. A loss of SE under compression along [111] due to the plastic deformation was also observed in Ti–Ni SMA micro-pillars.[20]

Figures 3(a) and 3(b) depict the temperature evolutions of the SE curves for [100] and [110] pillars. The turning points on the stress–strain curves in Fig. 3, marked by bold arrows, correspond to the MT start stress, σ_{MT}. The dependences in Figs. 3(a) and 3(b) reveal that the temperature increment causes the following effects: (i) an increasing of σ_{MT}, (ii) a tendency toward disappearance of the stress hysteresis for the [100] pillar, and (iii) a decreasing of the minimum on the plateau-like anomaly down to its vanishing for the [110] pillar. The linear dependence of $\sigma_{MT}(T)$ for the [100] pillar is in correspondence with the Clausius–Clapeyron equation.[1,8,19] Its estimated slope is of 1.8 MPa/K, which is smaller than 2.7 MPa/K for the bulk Ni–Fe(Co)–Ga [100] sample with the similar composition.[3] The $\sigma_{MT}(T)$ function for the [110] pillar does not show a linear behavior [Fig. 3(c)]. Note that in the bulk SMAs, exhibiting a tetragonal martensite with c/a > 1, the $\sigma_{MT}(T)$ compression dependences measured along [100] or [110] directions are straight lines with the same slope,[8] which can be hardly proved for the studied pillars. The aforementioned reduced value of the slope for the [100] pillar and/or the nonlinear behavior along [110] axis of the $\sigma_{MT}(T)$ curves have not been known yet for the already published SMA micropillars (because the temperature measurements were not available). The differences in the temperature dependences of the superelastic behavior of the bulk and micropillars can be tentatively attributed to the size effect. Further studies are necessary to uncover the underlying mechanisms behind this effect.

Bearing in mind the previously reported critical behaviors of the bulk Ni–Fe(Co)–Ga alloys,[3,4] we attribute the qualitative changes of the character of stress–strain curves as a function of the temperature in studied pillars (Fig. 3), cases (ii) and (iii), to the manifestation of the same criticalities. The aforementioned critical phenomena are related to the existence of CP on the austenite–martensite stress–temperature phase diagram similar to the case of critical effects in the liquid–gas phase diagram. In a critical point, where lability lines for martensite and austenite encounter, MT is terminated. Above CP, only postcritical behaviors are observed.[3,4] Here, we assume that a disappearance of stress hysteresis for the [100] pillar and vanishing of the minimum on the plateau-like anomaly for the [110] pillar in Figs. 3(a) and 3(b) are due to the existence of CPs on the stress–temperature phase diagrams plotted in Fig. 3(c),

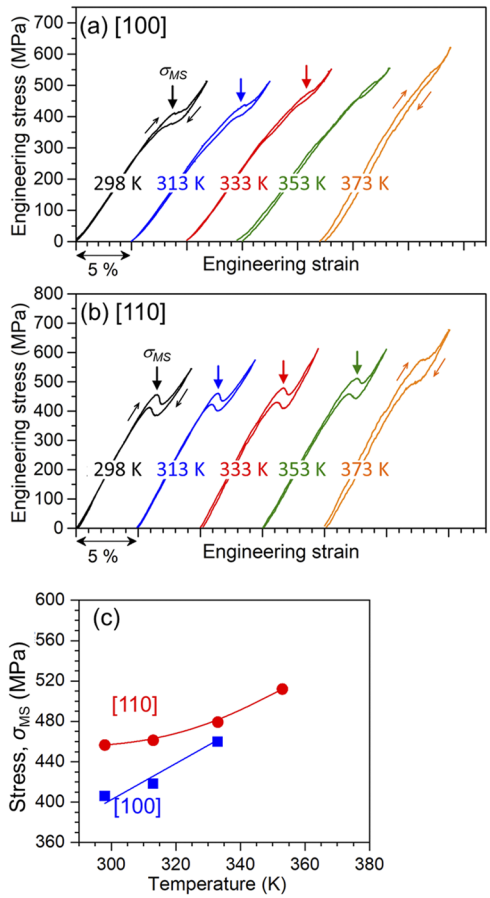

FIG. 3. Superelastic curves for (a) [100] and (b) [110] micropillars at different temperatures, and the vertical arrows indicate the martensite start stress (σ_{MS}). (c) σ_{MS} vs temperature phase diagrams of MT. Lines are guide to the eye.

so the stress–strain curves above 333 K for the [100] pillar and 353 K for the [110] pillar may correspond to the postcritical states. For the [100] pillar experiencing a disappearance of hysteresis, the location of CP coordinates on the phase diagram in Fig. 3(c) may be expected in the ranges 333 K < T^* < 353 K, 460 MPa < σ^* < 495 MPa. In the case of the [110] pillar still exhibiting a hysteresis above 353 K but no drop of stress on the plateau, we consider two arguments supporting a postcritical state: (a) MT disappears when the indications of the nonequilibrium processes due to its first-order character (drop of stress on the plateau) do not show up anymore, and (b) the persistence of stress hysteresis in the postcritical region may be explained by the time-dependent defect-produced mechanical losses.[4] With these arguments, the location of CP coordinates on the phase diagram for the [110] pillar in Fig. 3(c) may be expected in the ranges 353 K < T^* <373 K, 510 MPa < σ^* < 570 MPa. Figure 3 and the estimated CP coordinates confirm the orientation dependence of the CP location according to the known thermodynamic proportionality $\sigma^* \sim E_{[hkl]}$ (see Ref. 3 and Table I).

To conclude, this investigation on the microscale was mainly motivated by a discovery of the liquid–gas-type critical austenite–martensite phenomena along the stress–temperature phase diagram in the bulk Ni–Fe(Co)–Ga single crystals. In the present work, we have studied, for the first time, the temperature dependencies of the superelastic curves for the specially prepared Ni–Fe(Co)–Ga single crystalline micropillars. Such a study was instrumentally possible owing to the unique custom-made micro-compression setup equipped with the temperature stage. A huge linear deformation at room temperature, up to 10%, was found in the pillars as a result of the extremely low values of the Young modulus, which, in turn, has shown a dependence on the crystallographic orientation. The anomalous temperature evolutions of the micro-compression stress–strain curves have been interpreted as produced by the crystallographic-orientation-dependent critical behavior. The possible locations of the coordinates of the critical points (end points) on the stress–temperature phase diagrams of MT have been suggested for [100] and [110] pillars. Inasmuch as Ni–Fe(Co)–Ga, as one of the ferromagnetic shape memory alloys, exhibits a strong coupling between lattice strains and magnetic properties, further studies of magnetoelastic properties in a postcritical region on microscale would be very interesting not only for a basic science but also for the applications in novel microelectromechanical systems.

This work was supported by JST CREST, Grant No. JPMJCR1433, Japan, and the Grant-in-Aid for Scientific Research (S) (JSPS KAKENHI Grant No. 26220907), as well as by Spanish Ministry of Science, Innovations and Universities (Project No. RTI2018-094683-B-C53-54) and by the Basque Government Department of Education (Project No. IT1245-19).

DATA AVAILABILITY

The data that support the findings of this study are available from the corresponding authors upon reasonable request.

REFERENCES

[1] *Shape Memory Materials*, edited by K. Otsuka and C. M. Wayman (Cambridge University Press, Cambridge, 1998).
[2] T. Omori, M. Okano, and R. Kainuma, APL Mater. **1**, 032103 (2013).
[3] V. A. Chernenko, V. A. L'vov, S. Kabra, I. R. Aseguinolaza, M. Kohl, H. Hosoda, and J. M. Barandiaran, Phys. Status Solidi B **255**, 1700273 (2018).
[4] A. Kosogor, V. A. L'vov, V. A. Chernenko, E. Villa, J. M. Barandiaran, T. Fukuda, T. Terai, and T. Kakeshita, Acta Mater. **66**, 79 (2014).
[5] F. Lambrecht, N. Sagardiluz, M. Gueltig, I. R. Aseguinolaza, V. A. Chernenko, and M. Kohl, Appl. Phys. Lett. **110**, 213104 (2017).
[6] H. Ossmer, C. Chluba, S. Kauffmann-Weiss, E. Quandt, and M. Kohl, APL Mater. **4**, 064102 (2016).
[7] Y. Chumlyakov, E. Panchenko, I. Kireeva, I. Karaman, H. Sehitoglu, H. J. Maier, A. Tverdokhlebova, and A. Ovsyannikov, Mater. Sci. Eng. A **481-482**, 95 (2008).
[8] V. A. Chernenko, V. A. L'vov, J. Pons, and E. Cesari, J. Appl. Phys. **93**, 2394 (2003).
[9] Y. Chen and C. A. Schuh, Acta Mater. **59**, 537 (2011).
[10] J. F. Gómez-Cortés, M. L. Nó, I. López-Ferreño, J. Hernández-Saz, S. I. Molina, A. Chuvilin, and J. M. San Juan, Nat. Nanotechnol. **12**, 790 (2017).
[11] N. Ozdemir, I. Karaman, N. A. Mara, Y. I. Chumlyakov, and H. E. Karaca, Acta Mater. **60**, 5670 (2012).
[12] I. R. Aseguinolaza, E. Modin, A. Chuvilin, J. M. Barandiaran, and V. A. Chernenko, Appl. Mater. Today **12**, 9 (2018).
[13] K. Oikawa, R. Saito, K. Anzai, H. Ishikawa, Y. Sutou, T. Omori, A. Yoshikawa, V. A. Chernenko, S. Besseghini, A. Gambardella, R. Kainuma, and K. Ishida, Mater. Trans. **50**, 934 (2009).
[14] D. Kiener, P. Kaufmann, and A. M. Minor, Adv. Eng. Mater. **14**(11), 960 (2012).
[15] D. Kiener and A. M. Minor, Nano Lett. **11**, 3816 (2011).
[16] T. Nagoshi, T.-F. M. Chang, S. Tatsuo, and M. Sone, Microelectron. Eng. **110**, 270 (2013).
[17] K. Takashima, Y. Higo, S. Sugiura, and M. Shimojo, Mater. Trans. **42**, 68 (2001).
[18] T. Fukuda and T. Kakeshita, Scr. Mater. **69**, 89 (2013).
[19] V. A. L'vov, A. A. Rudenko, V. A. Chernenko, E. Cesari, J. Pons, and T. Kanomata, Mater. Trans. **46**, 790 (2005).
[20] C. P. Frick, S. Orso, and E. Arzt, Acta Mater. **55**, 3845 (2007).